A Novel Hierarchical Shape Analysis based on Sampling Point-Line Distance for Regular and Symmetry Shape Detection

Kehua Xian*
Department of Electro-mechanics and Information Engineering
Sichuan College of Architectural Technology
Sichuan, 618000, China

***Abstract*—Regular and symmetry shapes occurred in natural and manufactured objects. Detecting these shapes are essential and still tricky task in computer vision. This paper proposes a novel hierarchical shape detection (HiSD) method, which consists of circularity and roundness detection, and regularity and symmetry detection phases. The first phase recognizes the circular and elliptical shapes using aspect ratio and roundness measurements. The second phase, the main phase in the HiSD, recognizes the regular and symmetry shapes using density distribution measurement (DDM) and the proposed sampling point-line distance distribution (SPLDD) algorithm. The proposed method presets effective with low computation cost shape detection approach which is not sensitive to specific category of objects. It enables to detect different types of objects involving the arbitrary, regular, and symmetry shapes. Experimental results show that the proposed method performs well compared to the existing state-of-the-art algorithms.**

Keywords*—Shape recognition; hierarchical shape detection; sampling point-line distance distribution; regular and symmetry shape detection

I. Introduction

Regular and symmetry shapes occurred in the outdoor urban scenes, indoor built environments, and manufactured objects [1, 2, 24]. Detecting regular and symmetry shapes is essential in computer vision and pattern recognition communities. Regular and symmetry shape detection are broadly used in urban scene recognition [3, 4, 23], vehicle recognition [5, 6], face analysis [7, 8], image reconstruction [9], and driver assistance systems [10]. Moreover, the regular and symmetry shape features are considered salient features that guide eye movements and can thus mainly be used for visual attention detection [11].

Various methods have been developed for regular and symmetry shape detection. However, existing research works suffer from high complexity and it leads to deduct its applicability on real time shape detection applications [22]. As shown in literature, more existing methods focused on regular shapes detection which are limited to detect specific shapes such as circles or polygons. Moreover, these methods cannot detect symmetric shapes and differentiation from regular shapes.

Although many research works investigated regular shapes, the detection of polygon-based shapes has been studied less, and little progress has been made in recent years [3]. Barnes and Loy [4] presented a posteriori probability approach that defined the continuous log-likelihood of the probability density function for the appearance of regular polygons. Liu and Wang [3] introduced point-line distance distribution (PLDD) to compute each pixel's shape energy for detecting arbitrary triangles, regular polygons, and circles. Among the existing shape detection methods, the PLDD method [3] presented a better performance in terms of accuracy than other existing methods. However, the PLDD method suffers several drawbacks. The main drawback of the PLDD method is the lack of ability to identify symmetry and parallelogram format shapes [3].

Referring to existing drawbacks of current shape detection methods, developing an efficient with low complexity visual shape detection method is required to cover various shapes detection consisting regular and symmetry and other shapes. Therefore, this study presents a novel shape detection method to deal with the challenges, to detect different types of shapes, including the arbitrary, regular, and symmetry shapes with effective performance and low complexity.

The main contributions of this study are as follows, 1) a novel shape detection method developed which is not sensitive to specific category of objects. It enables to detect different types of objects involving the arbitrary, regular, and symmetry shapes, 2) the proposed method is not based on high complexity and computation cost approaches which is applicable in real time applications, 3) the experiments and comparative analyses are performed using different shapes and noise conditions to validate the effectiveness of the proposed method.

The rest of this paper organizes as follows: related methods and the existing shape detection methods are briefly reviewed in Section II. The proposed shape detection method is described in Section III. Section IV presents the experimental results and performance evaluation. Finally, Section V presents the conclusion of the paper. Hierarchical Shape Detection (HiSD) Method.

II. Related Works

This section discusses existing research works on shape detection methods. The standard and symmetry shape detection methods are categorized into deterministic-based and

*Corresponding Author.

stochastic-based approaches [3]. For the deterministic-based approaches, Hough transform-based methods are commonly applied to infer the center locations, followed by employing edge information obtained by an edge detector [12]. However, the Hough transform-based methods require large storage space and high computational complexity, which results in low processing efficiency. Furthermore, template matching [13] and least square-based methods have been proposed [14] for the discriminative-based approach. For the stochastic-based methods, Dehmeshki and Ye [15] proposed a Genetic Algorithm (GA)-based method for shape recognition that effectively detects regular shapes. However, the GA-based method cannot differentiate the regular and symmetry shapes. Furthermore, other stochastic-based methods have been proposed based on the random sample consensus technique [16] and simulated annealing [17].

III. The Proposed Method

The proposed shape detection method in this study consists of two main processes, which are hierarchically structured, as shown in Fig. 1. The first process calculates the roundness and circularity of the shape to identify whether the shape is a circle, ellipse, or not circular. The second and main process aims to detect the regularity and symmetry of the shapes.

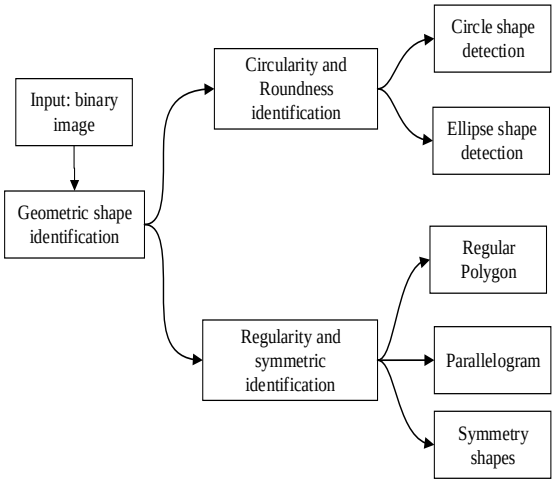

Fig. 1. The Hierarchical Shape Detection Method.

A. Circularity and Roundness Identification

Aspect ratio (*AR*) and roundness factors are used to detect the circularity of the shape. The *AR* is defined as the ratio of length over breadth [18]. *AR* can be calculated through Equation (1) as,

$$\mathrm{AR} = \frac{\mathrm{L}}{\mathrm{B}} \quad (1)$$

where *L* and *B* are the length and breadth of the shape, respectively. Moreover, the roundness feature describes the shape's resemblance to a circle. The roundness factor of a shape will approach 1.0, the closer the shape resembles a circle [18]. The roundness factor (*Ro*) can be obtained by Equation (2),

$$Ro = \frac{1}{\pi}\left(\frac{4*EA}{((D))^2}\right) \quad (2)$$

where *EA* is the enclosed area of the shape and *D* is the diameter.

B. Regularity and Symmetry Identification

This section describes a proposed algorithm to distinguish the shape based on regularity, irregularity, symmetric and asymmetric features. The pseudocode of irregularity and symmetric identification is as follows

***Input**: a binary component denotes as S.*
1- *Extract a corner point as P_c from S,*
2- *Compute angles as θ_k for each P_c using Equation (4),*
3- *Determine equal P_c points, initialize N_{eq} and detect shape regularity of S and update the S(T) function,*
4- *For each two connected P_c do:*
   a. *Find mean point as P_m,*
   b. *Generate a perpendicular line as BL that cross the P_m,*
   c. *Measuring the density distribution for two side of BL using calculate integral of are mass based Equation (9) and update symmetry status,*
   d. *Access the symmetry status of the using SPLDD and update symmetry status,*
5- *Distinguish the shape using obtained status*

***Output**: shape detection results*

1) Corner points extraction: A corner point is an edge point that occurs when the edge direction changes. In this study, features from the accelerated segment test (FAST) corner detector are used to extract the corner points [19]. FAST corner detector uses a circle of 16 pixels to classify whether a candidate point p is a corner, as presented in [19]. Each pixel in the circle is labeled from integer 1 to 16 clockwise. Suppose a set of N contiguous pixels in the circle are all brighter than the intensity of candidate pixel p (denoted by Ip) plus a threshold value t or all darker than the intensity of candidate pixel p minus threshold value t. In that case, p is classified as a corner. In a mathematic demonstration, for each location on the circle x, the pixel at that position relative to p (denoted by $p \rightarrow x$) can have one of three states by Equation:

$$S_{p\to x} = \{d, \quad I_{p\to x} < I_p - t \quad (darker)\ d, \quad I_p - t < I_{p\to x} < I_p + t \quad (similar)\ b, \quad I_p + t \le I_{p\to x} \quad (brighter) \quad (3)$$

Choosing an *x* and computing $Sp{\to}x$ for all $p \in P$ (the set of all pixels in all training images) partitions *P* into three subsets, *Pd, Ps, and Pb*, where each *p* is assigned to [19]. As an example, a pentagon is used to demonstrate the steps. The FAST corner detector can detect the corners of the pentagon, as shown in Fig. 2.

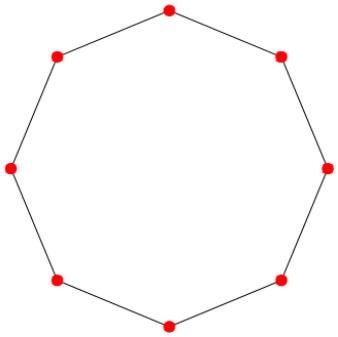

Fig. 2. Detected Corners of a Pentagon Shape.

2) Corners angles computation: As stated in the shape detection algorithm, the angle for each corner is required to identify. A scalar product-based approach is used for corer angle calculation. In this regard, a 5*5 mask is defined to identify the angle for the corner points. The mask is used for intersection point identification, obtained using corner points and sides on the shape. For this identification, the mask is located on the corner point, and the angle is calculated using the extraction of intersection points between the mask and the sides of the shape, as shown in Fig. 3 (P_c is the corner point and P_i, P_j are the intersection points on the shape sides). The mask contains 0 for all elements in M except M_{33} which is 1.

$$M = [0\ 0\ 0\ 0\ 0\ 0\ 0\ 0\ 0\ 0\ 0\ 0\ 1\ 0\ 0\ 0\ 0\ 0\ 0\ 0\ 0\ 0\ 0\ 0\ 0]$$

Let us define $P_c = (x_c, y_c)$ as a corner point, $P_i = (x_i, y_i)$ and $P_j = (x_j, y_j)$ as intersection points between mask (M) and polygon sides. The angle for corner point can be obtained using the scalar measurement [20],

$$\theta_k = arccos\left(\frac{\overrightarrow{P_iP_c}.\overrightarrow{P_cP_j}}{\|\overrightarrow{P_iP_c}\|\|\overrightarrow{P_cP_j}\|}\right) \quad (4)$$

where P_c denotes corner point, P_i and P_j denotes intersection points between mask and polygon sides.

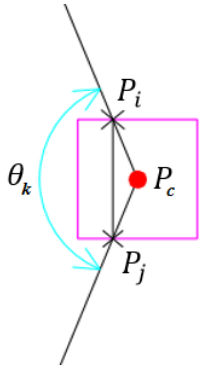

Fig. 3. The Corner Points (P_c) and Intersection Points (P_i, P_j) for Corner Angle Calculation (θ_k).

3) Shape regularity detection: After the corner angle computation, it is required to identify the regularity of the shape. In this regard, a function defines a rule as shown in Equation (5),

$$S(T) = \{(N_{eq} \cong N_T)\ and\ \left(\left(D(P_{c_i}) \cong D(P_{c_{i+1}})\right) \forall |u_{i\,N_T}\right) \rightarrow S \in Regular \quad \left(N_{eq} \cong 4\right)\ and\ \left(N_{eq} \cong \left[\frac{N_{eq}}{2}\right]\right) \rightarrow S \in parallelogram \quad (5)$$

According the function definition, *S(T)* is defined as the function for determination of shape type. The types of the shape type are regular or parallelogram. This type can be identified using a number of equal angle corners (N_{eq}). As the first statement in *S(T)*, If the N_{eq} is approximately equal to total number of corner (N_T) and the distances between corner points are roughly equal, the shape determined as regular shape. Otherwise, if the number of equal angle corners is approximately equal to four and half number of equal angle corners, the shape is determined as a parallelogram.

Euclidean distance is used for the distance measurement of corner points. For instance, the Euclidean distance between *i-th* corner points as P_{c_i} and its neighbor as $P_{c_{i+1}}$is calculated and denotes as $D(P_{c_i})$. Furthermore, a shape is detected as a parallelogram when N_{eq} is equal to a minimum number of $N_T/2$. For example, Fig. 4 shows a regular polygon shape in which the number of equal corners is equivalent to the number of total corners points, and the distances between all the corner points are the same.

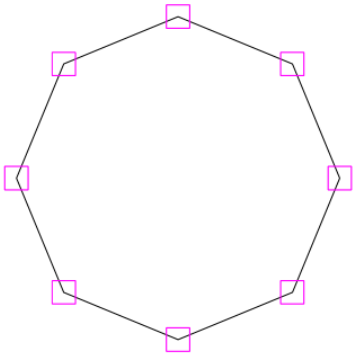

Fig. 4. A Regular Polygon with Same Number of Equal Corners and the Distances between the Corner Points.

4) Symmetry shape detection: Sometimes the shape is not detected as regular and parallelogram. In this case, the symmetric feature of the shape is checked. Fig. 5 illustrates a non-regular symmetric shape.

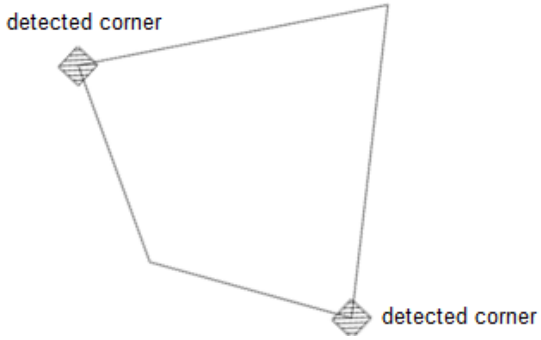

Fig. 5. Illustration of a Symmetric Shape.

In the first step, two corresponding corner points are connected through a line, and the mean point of this line is determined P_m. Based on identified P_m, a perpendicular line is drawn and named baseline *(BL)*. Using the *BL*, two correspondence corner points are identified. The length of *BL* is denoted as L_{bl}, which is measured by measuring the longest line connecting the two farthest points from the *S* perimeter. Furthermore, the details of the algorithm are demonstrated in a synthetic symmetry and asymmetry shape as shown in Fig. 6 and Fig. 7.

a) Density Distribution Measurement (DDM)

The *BL* is devised the *S* into two sections (it is called two sides in a shape which is divided in terms of on *BL*). The individual side is defined as a density function as *f (x, y)*. The *DDM* of both sides of the shape is calculated to measure the area side. The *DDM* is based on calculating integral under each space of *BL* sides. A density distribution function using a two-dimensional Cartesian moment m_{pq}, is the order of $p + q$, as *f (x, y)*, can be defined as,

$$m_{pq} = \int_{-\infty}^{\infty} \int_{-\infty}^{\infty} x^p y^p f(x,y)\, dx\, dy \quad (6)$$

The two-dimensional moment for a ($N \times M$) discretized image, *g (x, y)*, is:

$$m_{pq} = \sum_{y=0}^{M-1} \sum_{x=0}^{N-1} x^p y^p\, g(x,y) \quad (7)$$

For a given intensity distribution g(x, y) the image moments is defined. A complete moment set of order n consists of all moments m, such that $p + q \leq n$ and contains *1 / 2(n +1) (n +2)* elements. The definition of the zeroth order moment of the distribution, f (x, y),

$$m_{00} = \int_{-\infty}^{\infty} \int_{-\infty}^{\infty} f(x,y)\, dx\, dy \quad (8)$$

where m_{00} represents the total mass of the given distribution function or section. The zeroth moment represents the total region area. Therefore, the mass of each side can be measured using zeroth moment. After measuring area mass for each side, the obtained values are compared to identify whether they are close or not. A threshold value defines an acceptable range for the obtained values area mass to distinguish the shape as symmetric.

Fig. 6 demonstrates the strategy of regularity and symmetry shape detection shape. As shown in the Fig. 6, the corners of the shape are firstly detected. Secondly, mean metric is calculated using Euclidian distance for each corner pairs as shown in Fig. 6(b). Then a base-line between each corresponding corner points are drawn which intends to divide two are of region for each generated sides of the base-line as shown in Fig. 6(c). Finally, area feature is calculated for each region to check the equality of them. Similar to Fig. 6, the furthest corners of the shape are detected in first step. Then base-line and area region are considered for symmetry measurement and identification.

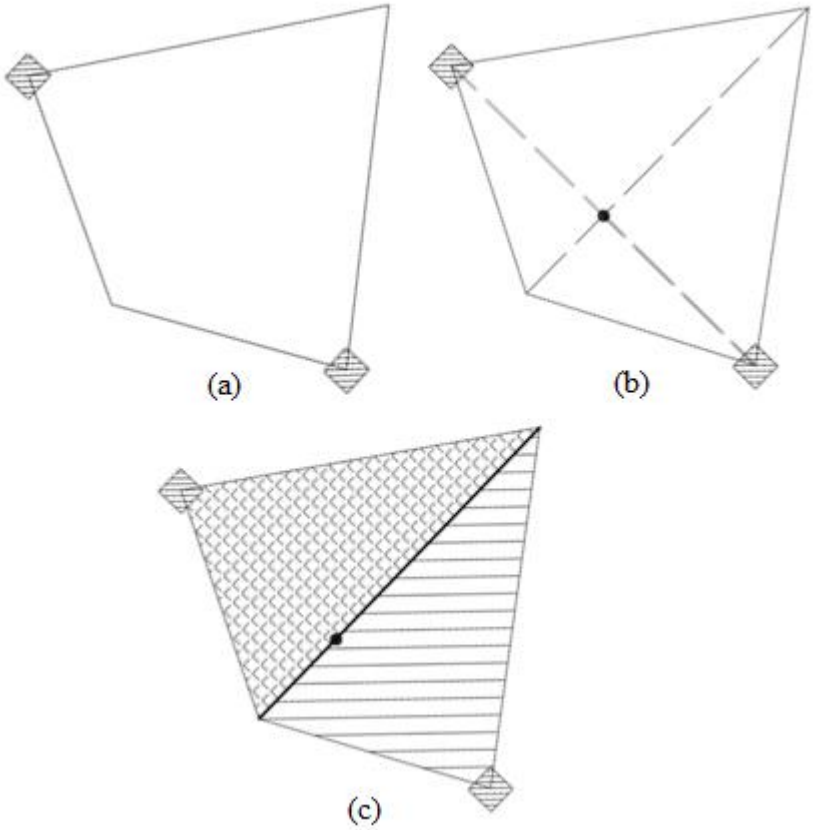

Fig. 6. Demonstration of Shape Regularity and Symmetric Identification for a Symmetric Shape. (a): Detected Corner, (b): Obtain Mean between Two Corner Points (P_m), (c): Calculate the Area for Region of each Sides.

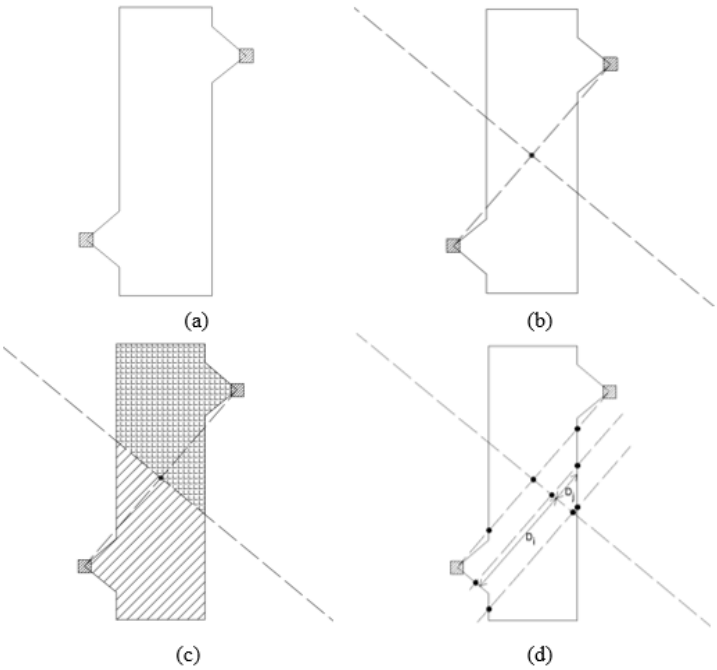

Fig. 7. The Process for Asymmetric Shape Identification.

b) Sampling Point-Line Distance Distribution (SPLDD)

Based on the DDM process, most of the shapes can be detected for symmetry shape identification. However, in some cases like Fig. 7, although the area for two sides of *BL* (the output of the DDM process) are quite similar, they are not symmetric shapes. Meanwhile, using the DDM, they are detected as symmetric shapes though they are not symmetrical.

Our shape detection method considers an algorithm to deal with the *DDM* challenge. The proposed algorithm is adopted from the point line distance distribution (*PLDD*) algorithm [3]. This algorithm is improved with sampling consideration in the *PLDD* algorithm and named Sampling Point-line Distance Distribution (*SPLDD*). The steps of *SPLDD* are as follows: finding the mean point (*Pm*), generating the baseline (*BL*), evaluating the area located on both side of *BL*.

In the *SPLDD* algorithm, as shown in Fig. 8, a set of sample points as P_s are generated on *BL*. In order to generate the P_s points, it is necessary to identify how many P_s are required to allocate on *BL*. For a number of sample points' identification, the length of *BL* (L_{bl}) is considered. Number of P_s denotes as ∂. Different values are tested for ∂ to find the optimum value. In this study, the value of ∂ is identified experimentally, which is $\partial = 10$. Using the value of ∂, the sample points (P_s) are generated. These points are used to draw confluence lines (*CL*). The confluence lines *(CL)* are defined to find the intersection points on *BL*. The *CL* lines touch the sides of the shape *(S)* to find the intersection points around the shape. The intersection points from the *CL* lines are marked as confluences points *(CP)*. Fig. 8 illustrates the details of the proposed *SPLDD* algorithm.

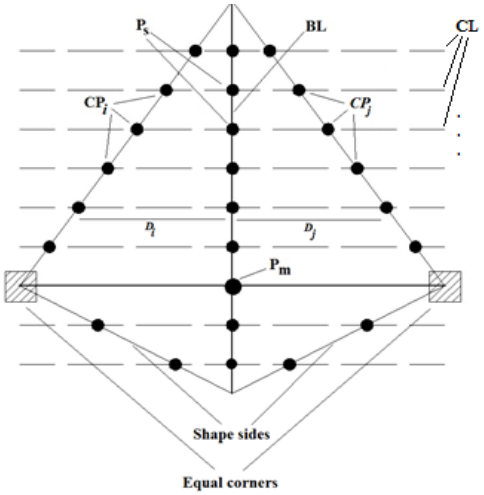

Fig. 8. Graphical Demonstration of *SPLDD* Algorithm.

Since the *CL* lines have an intersection in two opposite sites, two individual points (*CP)* are defined as $CP_i\ (x_i, y_i)$, $CP_j\ (x_j, y_j)$. The *CL* lines cross P_s point that defines as $P_s\ (x_s, y_s)$. The distance between P_s, CP_i and P_s, CP_j (these points are located on a *CL*) are calculated and denoted as D_i and D_j are calculated. This distance measurement uses a Euclidean distance measurement with the following equations,

$$d_i(X) = \sqrt{(x_s - x_i)^2 + \left(y_s - y_{ij}\right)^2},\ d_j(Y) = \sqrt{\left(x_s - x_j\right)^2 + \left(y_s - y_j\right)^2} \quad (9)$$

where the $d(x)$ and $d(y)$ are calculated individually for three points associated with *CL*, however, it is required to perform the distance measurements for all *CP* and *CL*. In this regard, two individual matrices are defined to store all the distance measurements:

$$D(X) = (d_1\ (X)\ d_2\ (X)\ d_3\ (X)\ \vdots\ d_n\ (X)\ )$$
$$D(Y) = (d_1(Y)\ d_2(Y)\ d_3(Y)\ \vdots\ d_n(Y)\ ) \quad (10)$$

where $d(X)$ and $d(Y)$ contains all the distances between the *CP* and P_s points those are located on the associated *CL*. Using Equation (11), the elements from a matrix are compared to the corresponding distance from another matrix. Consequently, based on the distance comparison, the equal distance of elements is identified, and corresponding points are labeled as True Points (*TP*).

$$\forall\left(d_k\ (X) \in D(X)\ , d_k\ (Y) \in D(Y)\right) \quad (11)$$

$$TP(p_s) = \{\ p_s \to true, \quad d_k\ (X) \approx\ d_k\ (Y),\ \ p_s \to false, \quad d_k\ (X) \approx\ d_k\ (Y)$$

where the function $TP(p_s)$ contains the true points labeled of p_s points. $d_k\ (X)$ and $d_k\ (Y)$ the distance measurements from $d(X)$ and $d(Y)$ matrices. Finally, a number of true points are counted to recognize whether the shape is symmetry or asymmetry. If the number of true points is equal to a defined threshold value, the shape recognizes as symmetry; else, it is asymmetry.

C. Experimental Results and Performance Evaluation

This section presents the experimental results and performance evaluation for the proposed method. For experiments, sample images are firstly generated using addition and applying some image processing operators, including noise and blurring. Secondly, two measurements: the number of correct and false detection variables, are used to measure the performance of the proposed method. Then, the evaluation analysis of the experimental results is presented. The evaluation analysis consists of performance and processing-time measurements.

As mentioned earlier, the sample images are generated based on PLDD experiments [3] for the shape detection experiments. For all the sample images, an image consists of different types of shapes (including regular and symmetry shapes): circles, squares, and regular triangles. Furthermore, for the sample images, Gaussian noise, Pepper & Salt noise, Gaussian blur, and JEPG compression are applied to generate the images for experiments. The generated sample images are organized into different categories-based range of noises scale and compression ratio, as shown in Table I. For example, two generated sample images from Gaussian noise and blur categories are shown in Fig. 9.

TABLE I. GENERATED OF SAMPLE IMAGES UNDER DIFFERENT CATEGORIES

Category	Operator type	Parameter	Range
1	Gaussian noises	Noise variation	0.01–0.04
2	Pepper & Salt noise	Noise density	0.01–0.06
3	Gaussian blur	Scale	0.5 to 3
4	JPEG compressed image	Compression ratio	from 1.33 to 6.02

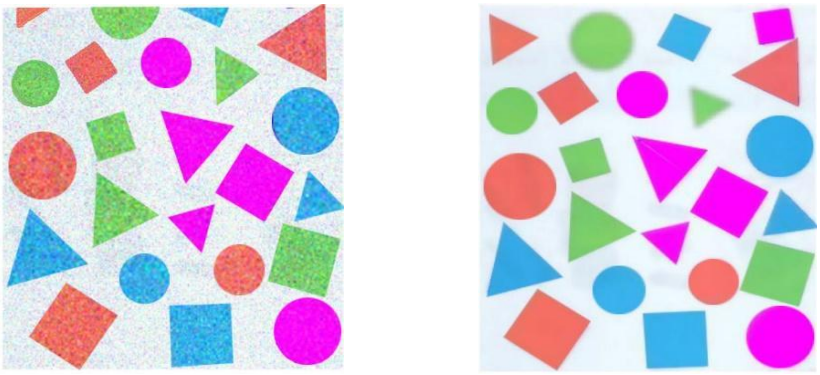

(a) (b)

Fig. 9. The Images from Dataset for Shape Detection Experiments and Evaluation (a) Gaussian Noise (Variance = 0.01), (b) Gaussian Blur (Scale = 2.5) [3].

D. Performance Evaluation

This section presents the performance evaluation for the proposed shape detection method. As presented in [3], two measurements are used to evaluate the performance. The measurements are the number of corrected shapes (*CN*) (true detection) and the number of false ones (*FN*) (false detection). The sum of the *CN* and *FN* are calculated using Equations (12) and (12),

$$CN = \sum_{i=1}^{N} \quad N_T$$

$$FN = \sum_{i=1}^{N} \quad N_F \tag{12}$$

$$Acc = \sum_{i=1}^{N} \quad \frac{CN}{CN+FN}, \tag{13}$$

where N_T and N_F are represented for true and false measurements. The *Acc* denotes accuracy measurement. The measurements are applied in the dataset containing the generated sample images considering defined noise categories, as shown in Table I. Then, the obtained results from the proposed method are compared to other methods, including the PLDD [3] and radial symmetry nature and direction-discriminated voting (RSNDV) [21] method, as shown in Table II.

As shown in Table II and Table III, in the noises categories, including Gaussian and Pepper & Salt noises, all methods, with increasing noises, the performance would be decreased due to decrease true detection and increased false detection. Based on the comparison, the proposed method achieved higher performance than other methods. The PLDD method also presented better performance when compared to the RSNDV method. The poor performance is because the method uses contour points for shape detection. The RSNDV method may miss some corner points that lead to false detection of shapes.

As shown in Table IV, in contrast to other categories, for both CN and FN measurements, the RSNDV method is the prior method compared to the proposed and PLDD methods. The reason for this can be using the voting approach and contour points features for shape detection in the RSNDV method. Using these features, the shape detector (RSNDV method) can detect shapes more accurately. However, in noise categories, the results are not the same with blur cases.

As shown in Table V, the proposed method roughly achieved better performance than other methods. In high ratio compression, the RSNDV method achieved higher performance in a number of correct shape detection; meanwhile, the PLDD and our proposed method archived promising results in lower compression ratio. However, with a lower compression ratio, our proposed method presented a better performance in false detection. Furthermore, the average processing time for the categories is calculated, and a comparison between our proposed method and other methods is illustrated. To calculate the average processing time, Equation (14) is used,

$$T_a = \frac{1}{N}\sum_{i=1}^{N} \quad T_i \tag{14}$$

where T_a indicates the average processing time for each category, an individual category's processing time (for example, the processing time for each Gaussian noise), and the number of experiments for each category. Table VI shows the comparison of average processing time for PLDD [3], RSNDV method, and the proposed method.

The processing time presented in Table VI for PLDD and RNSDV is based on Liu and Wang's [3] work. As shown in Table VI, the processing time is significantly reduced to be helpful in real-time applications. It is achieved by using the new SPLDD method, which is based on a sampling of points between the corner points instead of whole contour information.

TABLE II. PERFORMANCE COMPARISON BASED ON GAUSSIAN NOISE (CATEGORY 1)

Methods		**Noise Range**						***Acc***
		0.01	0.02	0.025	0.03	0.035	0.04	
PLDD	CN	24	24	23	21	21	18	0.86
	FN	0	2	3	4	4	7	
RSNDV	CN	23	21	23	20	18	19	0.62
	FN	1	10	4	13	27	20	
HiSD	CN	24	23	23	22	20	20	0.92
	FN	0	1	1	2	2	4	

TABLE III. PERFORMANCE COMPARISON BASED ON SALT & PEPPER NOISE (CATEGORY 2)

Methods		**Noise Range**						***Acc***
		0.01	0.02	0.03	0.04	0.05	0.06	
PLDD	CN	24	24	23	22	21	19	0.87
	FN	0	0	3	3	8	5	
Gang	CN	24	24	23	23	20	21	0.79
	FN	0	01	3	8	9	14	
HiSD	CN	24	24	23	23	21	20	0.88
	FN	0	0	2	4	6	7	

TABLE IV. PERFORMANCE COMPARISON BASED ON GAUSSIAN BLUR (CATEGORY 3)

Methods		**Blur Variation Range**						***Acc***
		0.5	1	1.5	2	2.5	3	
PLDD	CN	24	24	22	22	22	22	0.94
	FN	0	0	2	2	2	2	
RSNDV	CN	24	23	24	24	24	24	0.99
	FN	0	1	0	0	0	0	
HiSD	CN	24	24	23	23	23	23	0.93
	FN	0	0	1	2	3	3	

TABLE V. PERFORMANCE COMPARISON BASED ON JPEG COMPRESSION (CATEGORY 4)

Methods		**Ratio Variable**					***Acc***
		1.33	2.14	2.95	4.88	6.02	
PLDD	CN	24	24	24	23	14	0.90
	FN	0	0	0	2	10	
RSNDV	CN	22	23	24	21	21	0.91
	FN	2	1	0	3	6	
HiSD	CN	24	24	24	23	20	0.95
	FN	0	0	0	1	4	

TABLE VI. COMPARISON OF AVERAGE PROCESSING TIME FOR PLDD, RSNDV METHOD AND THE PROPOSED METHOD (IN TERMS OF SECONDS (S))

8	Gaussian noise	Pepper & Salt	Gaussian blur	JPEG compression
PLDD	24.39	26.73	24.29	25.27
RSNDV	163.68	146.48	70.58	88.77
HiSD	3.21	4.74	3.98	4.43

IV. CONCLUSION

This paper presented a shape detection method based on hierarchical and sampling point line distance distribution algorithms. The fundamental concepts of different shapes are first defined. The existing shape detection methods are reviewed, and the recent and relevant study is addressed. Based on the literature review, the PLDD method has shown promising results in arbitrary and regular shape detection. However, this method suffers from some challenges, such as a lack of efficiency in shape detection in different types, including rotationally convex symmetry, ellipse, and parallelogram. Therefore, this study proposed a new shape detection method called hierarchical shape detection (HiSD) to detect the shapes in hierarchical processes. In HiSD, a new algorithm with consideration of sampling point line distance distribution (SPLDD) algorithm was proposed to deal with PLDD challenges. The proposed shape detection method is not sensitive to specific category of objects. It enables to detect different types of objects involving the arbitrary, regular, and symmetry shapes. Furthermore, the proposed method is not based on high complexity and computation cost approaches which is applicable in real time applications. The experiments and comparative analyses are performed using different shapes and noise conditions to validate the effectiveness of the proposed method. The experimental results showed that the proposed shape detection method enables detection of different types of shapes, including circle, eclipse, regular, and symmetry shapes in different noise condition scenarios. For future works, this proposed method can be extended for irregular shape detection as they typically exist in real environment. Moreover, the proposed system can be implemented in real-time shape detection to extend the application of current research work.

REFERENCES

[1] Akbar, H., et al., Bilateral symmetry detection on the basis of Scale Invariant Feature Transform. PloS one, 2014. 9(8): p. e103561.

[2] Korman, S., et al. Probably approximately symmetric: Fast rigid symmetry detection with global guarantees. in Computer Graphics Forum. 2015. Wiley Online Library.

[3] Liu, H. and Z. Wang, PLDD: Point-lines distance distribution for detection of arbitrary triangles, regular polygons and circles. Journal of Visual Communication and Image Representation, 2014. 25(2): p. 273-284.

[4] Barnes, N., G. Loy, and D. Shaw, The regular polygon detector. Pattern Recognition, 2010. 43(3): p. 592-602.

[5] Teoh, S.S. and T. Bräunl, Symmetry-based monocular vehicle detection system. Machine Vision and Applications, 2012. 23(5): p. 831-842.

[6] Hsieh, J.-W., L.-C. Chen, and D.-Y. Chen, Symmetrical surf and its applications to vehicle detection and vehicle make and model recognition. Intelligent Transportation Systems, IEEE Transactions on, 2014. 15(1): p. 6-20.

[7] Xu, Y., et al., Approximately symmetrical face images for image preprocessing in face recognition and sparse representation based classification. Pattern Recognition, 2016. 54: p. 68-82.

[8] Saha, S. and S. Bandyopadhyay. A symmetry based face detection technique. in Proceedings of the IEEE WIE National Symposium on Emerging Technologies. 2007.

[9] Chou, C.-Y., et al., Accelerating Image Reconstruction in Dual-Head PET System by GPU and Symmetry Properties. PloS one, 2012. 7(12): p. e50540.

[10] Loy, G. and N. Barnes. Fast shape-based road sign detection for a driver assistance system. in Intelligent Robots and Systems, 2004.(IROS 2004). Proceedings. 2004 IEEE/RSJ International Conference on. 2004. IEEE.

[11] Kootstra, G., A. Nederveen, and B. De Boer. *Paying attention to symmetry*. in *British Machine Vision Conference (BMVC2008)*. 2008. The British Machine Vision Association and Society for Pattern Recognition.

[12] Kiryati, N., H. Kälviäinen, and S. Alaoutinen, *Randomized or probabilistic Hough transform: unified performance evaluation.* Pattern Recognition Letters, 2000. 21(13): p. 1157-1164.

[13] Qi, H., et al., An effective solution for trademark image retrieval by combining shape description and feature matching. Pattern Recognition, 2010. 43(6): p. 2017-2027.

[14] Chaudhuri, D., A simple least squares method for fitting of ellipses and circles depends on border points of a two-tone image and their 3-D extensions. Pattern Recognition Letters, 2010. 31(9): p. 818-829.

[15] Dehmeshki, J., et al., *Automated detection of lung nodules in CT images using shape-based genetic algorithm.* Computerized Medical Imaging and Graphics, 2007. 31(6): p. 408-417.

[16] Fischler, M.A. and R.C. Bolles, Random sample consensus: a paradigm for model fitting with applications to image analysis and automated cartography. Communications of the ACM, 1981. 24(6): p. 381-395.

[17] Birbil, Ş.İ., S.-C. Fang, and R.-L. Sheu, *On the convergence of a population-based global optimization algorithm.* Journal of global optimization, 2004. 30(2-3): p. 301-318.

[18] Image Metrology, S. *Shape Measurement Parameters*. 2015 15 Feb 2016]; Available from: http://www.imagemet.com/WebHelp6/Default.htm#PnPParameters/Measure_Shape_Parameters.htm.

[19] Rosten, E. and T. Drummond, Machine learning for high-speed corner detection, in Computer Vision–ECCV 2006. 2006, Springer. p. 430-443.

[20] Proofwiki. *Angle Between Vectors in Terms of Dot Product*. 2015; Available from: https://proofwiki.org/wiki/Angle_Between_Vectors_in_Terms_of_Dot_Product.

[21] Gang, W., et al. A Shape Detection Method Based on the Radial Symmetry Nature and Direction-Discriminated Voting. in Image Processing, 2007. ICIP 2007. IEEE International Conference on. 2007.

[22] Rampone, G., Makin, A.D., Tyson-Carr, J. and Bertamini, M., 2021. Spinning objects and partial occlusion: Smart neural responses to symmetry. Vision research, 188, pp.1-9.

[23] Xu, J., Cao, W., Liu, B. and Jiang, K., 2021. Object restoration based on extrinsic reflective symmetry plane detection. The Visual Computer, pp.1-16.

[24] Bartalucci, C., Furferi, R., Governi, L. and Volpe, Y., 2018. A survey of methods for symmetry detection on 3d high point density models in biomedicine. Symmetry, 10(7), p.263.